A triple solar desalination system integrated with a biomass-fuelled SCO2 power cycle: Thermodynamic modelling

Hamed Ghiasirad[a,*], Towhid Gholizadeh[b], Saeed Rostami[c], Bartosz Stanek[d], Anna Skorek-Osikowska[e], and Lukasz Bartela[f]

[a] *Silesian University of Technology, Gliwice, Poland, hamed.ghiasirad@polsl.pl*
[b] *Silesian University of Technology, Gliwice, Poland, Towhid.gholizadeh@gmail.com*
[c] *Sharif University of Technology, Tehran, Iran, rostami.sae@gmail.com*
[d] *Silesian University of Technology, Gliwice, Poland, bartosz.stanek@polsl.pl*
[e] *Silesian University of Technology, Gliwice, Poland, anna.skorek@polsl.pl*
[f] *Silesian University of Technology, Gliwice, Poland, Lukasz.bartela@polsl.pl*

Abstract:

Numerous methods are invented to capture the dissipating heat from different sectors, among all, the combination of power generation and fresh water units in the form of integrated systems based on renewable energy has received less attention. In traditional systems, not only was energy wasted to the environment, but fossil fuels caused serious damage to the environment. To overcome this problem, a new solar-biomass driven integrated system is devised in this investigation. Instead of wasting the energy of sCO2 into the environment, a novel system is proposed to increase EUF. Meanwhile, the use of HDH-TVC-RO along with the MED unit increases the amount of freshwater rate. The results indicated that the fresh water rate, GOR, and EUF are 29.36 kg/s, 14.38, and 3.372, respectively. Hence, the total GOR of the devised system is constant with the alteration of input vapor pressure to HDH-TVC; in contrast, the total GOR is increased with the increase of the pressure ratio of compressors. In addition, the behaviour of the EUF is linear in the presence of alteration of both parameters of input vapor pressure parameters to HDH-TVC and the pressure ratio of compressors.

Keywords:

Parabolic trough collector, biomass gasification, SCO2, MED desalination, HDH-TVC-RO.

1. Introduction

Water and power are two essential resources necessary for human survival and the functioning of modern society. Unfortunately, the scarcity of these resources is a growing concern worldwide, particularly in areas with growing populations, increased industrialization, and changing weather patterns. Access to clean and safe drinking water is a fundamental human right, yet many people in developing countries still lack primary access to this resource. Furthermore, power outages and unreliable energy sources can disrupt daily life, especially in countries with limited infrastructure. As the world population grows, there is an urgent need to address these issues and find sustainable solutions to ensure that everyone has access to these vital resources. On the other hand, the production of water and power with fossil fuels has significant environmental impacts that damage the planet. The combustion of fossil fuels releases carbon dioxide and other greenhouse gases into the atmosphere, contributing to global climate change [1]. In addition to climate change, extraction, transportation, and burning of fossil fuels can cause air and water pollution, habitat destruction, and soil degradation. For example, coal-fired power plants produce large amounts of air pollutants such as sulphur dioxide, nitrogen oxides, and particulate matter, contributing to respiratory problems and other health issues[2]. Production of water using fossil fuels can also lead to environmental degradation. Given these negative impacts, there is an urgent need to transition towards cleaner and more sustainable alternatives to produce water and power, such as renewable energy sources such as solar, wind, and biofuels.

Today, the use of Integrated Systems using renewable resources (ISRR) is a very efficient cure to overcome the problems of water and power shortage due to increased efficiency, cost savings, enhanced resilience, reduced environmental impact, and increased flexibility. Over the past decade, several investigations have pivoted the limelight on the all-round usage of the ISRR via proposing various renewable energies such as wind, solar and biofuels (for employing its producing heat) or recommending different thermal-driven

https://doi.org/10.52202/069564-0168

desalination systems (for producing drinking water). Xia et al. [3] proposed a solar-powered supercritical carbon dioxide (sCO_2) cycle for reverse osmosis (RO) desalination. The recommended integrated system includes a sCO_2 power cycle, solar collectors, RO, and LNG subsystem. They employed thermodynamics analysis and maximized the rate of produced drinking water by using a genetic algorithm for parametric optimization. They found an optimal value for the turbine input pressure of the sCO_2 cycle to obtain the maximum exergy efficiency. Under optimal conditions, a proposed ISRR reached the daily exergy efficiency of 4.90% and produced 2537.33 m^3 of drinking water per day. In 2016, Kouta et al. [4] conducted an investigation on ISRR comprised of a solar tower, a sCO_2 subsystem (for power generation), and multiple effect desalination with thermal vapor compression (MED-TVC) (for freshwater production). They compared two sCO2 cycles consisting of regeneration and recompression. ISRR was analysed from thermodynamic and exergoencomic points of view; the result showed that the solar tower generated more than 80% of the total entropy in both configurations, followed by the MED-TVC system, and the sCO_2 subsystem. A case study for different cities in Saudi Arabia was conducted and these results were extracted that the cities of Yanbu, Khabt, and Al-Ghusn achieved the lowest cost, respectively. The Yanbu LCOE was 0.0826 $/kWh and 0.0915 $/kWh for the recompression and regeneration solar cycles at a fraction of 0.5, respectively. Then, Sharan et al. [5] found the optimal feed flow in a cogeneration system consisting of a MED and sCO_2 for the production of electricity and freshwater simultaneously. The results showed that the forward feed is an optimum configuration compared to the parallel/ cross one. Consequently, the forward feed configuration reduced the distilled cost by 2.6% and increased the distilled production by 7.5%. In the same year, Alharbi et al. [6] compared two integrated systems consisting of sCO2 as a power supplier combined with multi-effect desalination coupled with mechanical vapor compression (MED-MVC) and conventional MED. Since the efficiency of the MED system is higher in the forward feed configuration[5], they invented both integrated systems with forward feed configuration. It was generally perceived that the performance of the conventional MED system in universal performance ratio, total water price, and specific power consumption for MED systems was better than that of the MED-MVC system. In 2019, Sharan et al. [7] invented an innovative concept to reduce the cost of distilled water. In this regard, they introduced an ISRR which includes a sCO_2 Brayton cycle that uses its dissipating heat to run a MED system. Concentrating solar power (CSP) plants were responsible for supplying energy to the integrated system. Due to the intermittency of solar radiation, the system included tanks for storing solar energy. Optimization of the storage tank led to reduction of the cost of distilled water by 19% and increase of the capacity of MED system from 46% to 75%. In addition, they compared the MED and RO systems from the point of view thermoeconomic, the comparison revealed that the use of MED can decrease the cost of distillation by 16%. In order to compare the distillation methods in the ISRR systems, Rostamzadeh et al. [8] conducted a cost comparison in two different ISRR systems. They juxtaposed the hybrid HDH-RO system and the solo-RO system, both of them driven by dissipating heat of the wind turbine. The results revealed that the drinking water production using a solo RO unit is cheaper than one using a hybrid HDH-RO desalination unit. Exergic analysis and operation simulations of the concentrated solar-driven power and desalination (CSPD) system are carried out by Wang et al. [9]. They showed that the efficiency of the sCO_2 cycle could be 36.6%, while the distilled water and output power produced by CSPD are 4050.8 t/day and 50.1 MW/day, respectively. In order of thermodynamic metrics, the results pointed out that two highest energy destruction and two minimum exergy efficiency are related to heat exchanger of the desalination system and solar tower receiver. They concluded that the CSPD systems are economically feasible since the system has levelized cost of water (LCOW) of 1.15 $/t and LCOE of 0.059 $/kWh. Since the use of sCO_2 can reduce the cost of solar power generation, Yuan et al. [10] used sCO_2 in the ISRR combined with the MED unit. One of the concerns about the combination of the sCO_2 cycle with the MED unit was the possibility of a decrease in the efficiency of the sCO_2 cycle, which they showed that such a combination does not reduce the efficiency of the sCO_2. They showed in the low split ratio (the ratio of the mass flow rate of the main compressor to the total mass flow rate), approximately less than 0.6, that the amount of freshwater produced decreases with the increase of the split ratio. For values greater than 0.6 the freshwater rate is increased with the increase in the split ratio. In the optimal state, the LCOE is 0.081 $/kWh and the LCOW is 0.81 $/$m^3$. Using the five-effect distillation system, the freshwater results indicated that the rate is 459 m^3/day. Realizing that the heat dissipating from an CSP-sCO_2 can be used for free but with slightly reduced thermal efficiency, Omar et al. [11] invented a new ISRR based on CSP, a CO_2 cycle, and Cascade MED system. The results indicated that four-MED systems can maximize freshwater production, with 57% dissipating heat energy recovery compared to 26% waste heat recovery using a single-MED system. In another study, khanmohammadi et al. [12] proposed an ISRR system consisting of a solar collector, a humidification and dehumidification (HDH) unit. The system is surveyed using environmental simulation and thermodynamic modelling. The results indicated that an increase in the compressor pressure ratio leads to a decrease in COP and freshwater flow. Similarly, freshwater production and exergy efficiency decrease with an increase in the outlet pressure. Although the authors used a solar collector to supply the heat needed for the HDH system, they could use a sCO_2 system to increase the efficiency of the system and supply the energy by using dissipating the heat of the sCO_2 unit.

The use of clean energy to prevent serious damage to the environment is not limited to solar and wind energy. In several scholars, attention has been paid to biomass to supply the heat needed for ISRR

https://doi.org/10.52202/069564-0168

consisting of the sCO_2 cycle. Balafkandeh et al. [13] proposed a biomass-based heating, power, and cooling system configuration consisting of sCO_2.The system was analysed from thermodynamic exergoeconomic viewpoints, in addition an environmental analysis is carried out to evaluate the CO_2 emission of the proposed system. Cao et al. [14] introduced a biomass-fueled integrated cycle to generate adequate power. The invented system includes two Brayton cycles with working fluids of sCO2 and nitrogen. An economic and thermodynamic investigation is performed. To seek the optimum from the exergoeconomic viewpoint, multi-criteria optimization is conducted. The results indicated that the exergetic efficiency reach 43.51% and the power cost leads 19.78 $/GJ in state of optimal point. Finally, in 2023, Hai et al. [15] combined a biomass-fueled SCO2 cycle with a MED desalination system to product power and freshwater simultaneously with the highest efficiency and without harming the environment.

1.1. Scientific Gaps

According to the authors of the above-reviewed works, it can be understated that there are considerable scientific gaps in previous studies dealing with the integration of the sCO_2 cycle with a desalination unit as a bottoming cycle for the production of power and drinking water, simultaneously. Although it has been shown in the above literature that various sources of clean energy including solar, wind and biomass can be used to supply the required heat of the bottoming cycle (e.g., MED unit), each of them has shortage. To date, no one has used the combination of two renewable resources for driving one of the desalination methods. It has been indicated that using the MED unit as the bottoming cycle of the sCO2 system driven by a biofueled heat source is carried out by Hai et al. [15]. However, they did not pay attention to the fact that the fresh water produced by the MED unit has a high temperature compared to the ambient temperature. In this case, by slightly increasing the temperature of the produced water, it can be used as an energy supplier in low-temperature cycles such as HDH unit. Furthermore, it is obvious that the drinking water distillated from a MED unit is more expensive than an HDH unit due to Khalilzadeh and Nezhad [16]reported a high value of 16.16 $/kWh for the cost of fresh water.

1.2. Novelties

Integration of the Rankine cycle with a distillation system can increase the operating pressure of the condenser (in the Rankine cycle), which leads to an increase in the heat-rejection temperature. Still, such a combination reduces the efficiency of the power plant's efficiency[5]. To eliminate the defect of reducing efficiency, it is possible to utilize the sCO_2 Brayton cycle because it has high efficiency compared to the Rankine cycle. On the other hand, the sCO_2 cycle has high-temperature rejection that is suitable for driving an MED system[7]. As mentioned, the biomass-fueled integration of the sCO_2 and MED unit was investigated in 2023. But in the present study, to increase the amount of freshwater production, the freshwater produced by the MED unit, which has a relatively high temperature, was redirected to a new subsystem consisting of HDH-TVC-RO. Solar collectors are used to increase the temperature of the redirected freshwater that drives the HDH-TVC-RO unit. All in all, the primary purpose of this study is multifaceted and is pinched as follows:

- Proposing a novel integrated system using biomass and solar energy as primary sources.
- Using MED, HDH, and RO desalination unit and sCO_2 cycle in the solar biomass-based multigeneration unit.
- investigating a comprehensive study assessing the impacts of vital parameters on the performance of the invented integrated system.

2. Description of the setup

A schematic diagram of the proposed system is shown in Fig. 1. The system consists of five subsystems: gasifier, supercritical CO2 cycle, Multi-effect desalination system, Parabolic Trough Solar and varied pressure humidification-dehumidification system coupled with reverse osmosis. In the gasification process, biomass (68) and environmental air (69) are fed to the gasifier where syngas is produced. Syngas is then fed to the combustion chamber (CC) together with the hot air exiting from the Air pre-heating (76). The high-temperature combustion products (71) are directed to the reactor to supply the energy for the supercritical CO2 cycle, which is used to increase the turbine inlet temperature (TIT) in the S–CO2 cycle (2). The SCO2 power cycle is actually a combination of the Power system and the MED (multi-effect desalination) so that the heat rejected in the gas cooler1 of the S–CO2 system is utilized to run the MED which is used to produce fresh water in the MED system.

Some of the water produced by the MED system increased pressure by the water pump (62). The high-pressure water then takes its initial energy through the PTC (Parabolic Trough Collector) system, and the high-pressure water is converted into steam by the evaporator, which obtains this energy from the exhaust gas. The high-pressure steam (46) by thermal vapor compressor enters a humidification-dehumidification system coupled with reverse osmosis to produce more water.

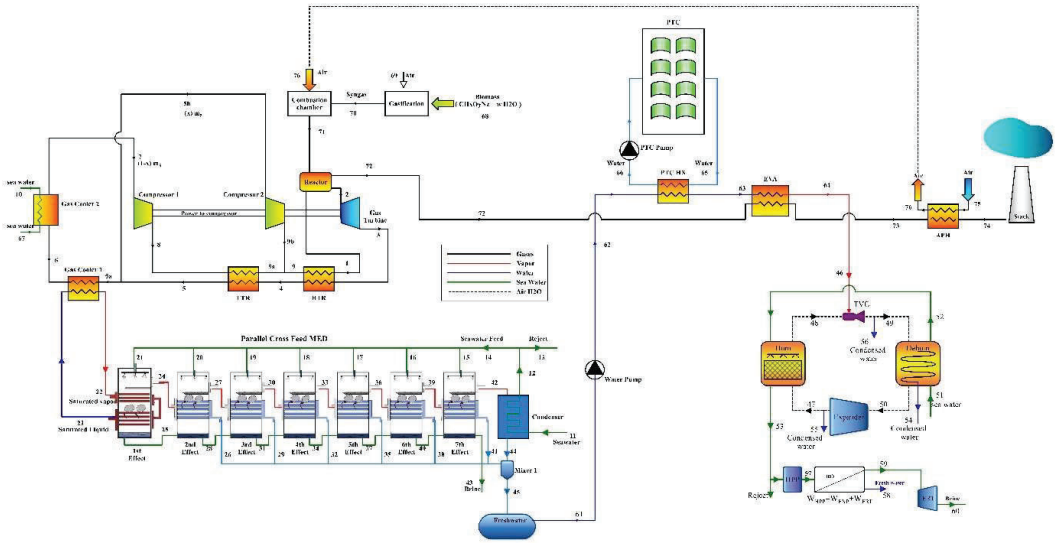

Figure 1: Schematic of the devised solar-biomass-driven power/desalination unit.

3. Materials and Methods

3.1. Thermodynamic assumptions

To analyse the proposed solar-biomass integrated system, below assumptions are developed:

- All Governing equations and thermodynamic process are advanced under steady-state condition.
- The freshwater temperature is assumed as the average temperature of the air in the closed loop of HDH unit.

In addition, other required thermodynamic data for the devised system is illustrated in Table 1.

Table 1: Set of input parameters for thermodynamic simulation of the devised system.

The input data	Unit	Value	Ref.
Ambient temperature	K	298.15	[17]
Ambient press	bar	1.013	[17]
Gasifier and combustion reactions			
Type of biomass feedstock		$Wood\ CH_{1.44}O_{0.66}$	[18]
Biomass flow rate	Kg, s^{-1}	1.115	[19]
Moisture content	%	20	[18]
Gasification temperature	K	1073.15	[18]
Outlet temperature of combustion chamber	K	1520	[20]
Pressure ratio of compressors		3	[21]
Temperature output of gas cooler 2	C	35	[22]
Temperature of Reactor	C	550	[21]
Compressor efficiency	%	0.9	[21]
Turbine efficiency	%	0.85	[21]
Epsilon LTR	%	0.86	[22]
Epsilon HTR	%	0.86	[22]
Pressure output Turbine	bar	74	[22]
Temperature difference of Gas cooler 1	C	10	[22]
Number of effects		7	[23]
Seawater salinity	gr/kg	35	[23]
Condensation temperature of the 1st effect	K	344.15	[23]
Temperature difference between effects	K	3.3	[24]
Temperature difference condenser	K	0.7	[24]
Feed/seawater mass flow rate ratio at states 13 and 14		0.415	[24]
Number of PTC		3	
Pressure of PTC water	bar	15	[25]

https://doi.org/10.52202/069564-0168

DNI ptc	W/m^2	1000	[25]
Fluid work		Water	[25]
Temperature difference PTC_hex	K	10	
Inlet Temp of PTC	C	70	[25]
Mass flow rate of PTC	Kg/s	0.8	[25]
Vapor Pressure inlet TVC	bar	50	[26]
Seawater salinity	g/kg	35	[27]
Humidifier effectiveness	%	85	[27]
Dehumidifier effectiveness	%	85	[27]
Expander efficiency	%	50	[26]
TVC efficiency	%	30	[26]
TVC pressure ratio		1.2	[26]
Pump efficiency	%	70	[27]
Heat capacity rate ratio		1	[26]
Recovery ratio	%	0.3	[28]
Salt rejection percentage		0.9944	[28]
Fouling factor		0.85	[28]
Element area	m^2	35.4	[28]
Number of elements		7	[28]
Number of pressure vessels		42	[28]

3.2. Energy analysis

Conservation equations including energy and mass can be articulated as [29]:

Mass balance Eq.:

$$\sum \dot{m}_{in} - \sum \dot{m}_{out} = 0 \tag{16}$$

Energy balance Eq.:

$$\dot{Q}_{c.v.} - \dot{W}_{c.v.} = \sum (\dot{m}h)_{out} - \sum (\dot{m}h)_{in} \tag{17}$$

Salinity balance Eq.:

$$\sum (\dot{m}S)_{in} - \sum (\dot{m}S)_{out} = 0 \tag{18}$$

The desalination flow ratio (MR) of the HDH unit is expressed as follows [23]:

$$MR = \frac{\dot{m}_{seawater}}{\dot{m}_{dryair}} \tag{19}$$

The effectiveness of humidifier/dehumidifier (ε) is expressed as below [23]:

$$\varepsilon = \frac{\Delta \dot{H}}{\Delta \dot{H}_{max}} \tag{20}$$

The energy, mass and salinity relations for each component of the invented system are showed in Table 2.

Table 2: Mass, Salinity, and Energy balance equations for each component of the proposed system.

Component	Mass and energy balance equations
Reactor	$\dot{Q}_{Rect} = \dot{m}_{71}(h_{71} - h_{72}) = \dot{m}_2(h_2 - h_1)$
Gas Turbine	$\dot{W}_{Gastur} = \dot{m}_2(h_2 - h_3), \quad \eta_{Gastur} = \frac{h_2 - h_3}{h_2 - h_{3S}}$
HTR	$\dot{Q}_{HTR} = \dot{m}_3(h_3 - h_4) = \dot{m}_1(h_9 - h_1)$
LTR	$\dot{Q}_{LTR} = \dot{m}_4(h_4 - h_5) = \dot{m}_8(h_9 - h_8)$
Compressor 1	$\dot{W}_{comp\,1} = \dot{m}_7(h_8 - h_7), \quad \eta_{comp\,1} = \frac{h_7 - h_{8S}}{h_7 - h_8}$
Compressor 2	$\dot{W}_{comp\,2} = (x)\dot{m}_5(h_9 - h_5), \quad \eta_{comp\,2} = \frac{h_5 - h_{9S}}{h_5 - h_9}$
Gas cooler 1	$\dot{Q}_{GC1} = \dot{m}_6(h_5 - h_6) = \dot{m}_{22}(h_{22} - h_{23})$
Gas cooler 2	$\dot{Q}_{GC2} = \dot{m}_6(h_6 - h_7) = \dot{m}_{10}(h_{67} - h_{10})$
Effects	$T_{V,out} = T_{\mathrm{B,out}} = T_{\mathrm{V,in}} - \Delta T_{Eff}$

	$\dot{m}_{\mathrm{SW}} + \dot{m}_{\mathrm{B,in}} = \dot{m}_{V,out} + \dot{m}_{\mathrm{B,out}}$ $\dot{m}_{B,in} S_{\mathrm{B,in}} + \dot{m}_{\mathrm{SW}} S_{\mathrm{SW}} = \dot{m}_{B,out} S_{\mathrm{B,out}}, \quad \dot{m}_{\mathrm{SW}} = \frac{\dot{m}_{14}}{N_{Eff}}$ $\dot{m}_{\mathrm{FW}} h_{\mathrm{FW}} + \dot{m}_{V,out} h_{V,out} + \dot{m}_{\mathrm{B,out}} h_{\mathrm{B,out}} = \dot{m}_{\mathrm{SW}} h_{\mathrm{SW}} + \dot{m}_{V,in} h_{V,in} + \dot{m}_{B,in} h_{\mathrm{B,in}}$
condenser	$\dot{Q}_{Cond} = \dot{m}_{12}(h_{12} - h_{11}) = \dot{m}_{42}(h_{42} - h_{44})$
Mixer	$\dot{m}_{26} h_{26} + \dot{m}_{29} h_{29} + \dot{m}_{32} h_{32} + \dot{m}_{35} h_{35} + \dot{m}_{38} h_{38} + \dot{m}_{41} h_{41} = \dot{m}_{45} h_{45}$
Water Pump	$\dot{W}_{WPump} = \dot{m}_{61}(h_{62} - h_{62}), \quad \eta_{WPump} = \frac{h_{61} - h_{62}}{h_{61} - h_{62S}}$
PTC HX	$\dot{Q}_{PTC,Hex} = \dot{m}_{62}(h_{63} - h_{62}) = \dot{m}_{65}(h_{65} - h_{66})$
Evaporator	$\dot{Q}_{Eva} = \dot{m}_{63}(h_{64} - h_{63}) = \dot{m}_{72}(h_{72} - h_{73})$
Air preheater	$\dot{Q}_{APH} = \dot{m}_{74}(h_{74} - h_{73}) = \dot{m}_{76}(h_{76} - h_{75})$
Dehumidifier	$\dot{m}_{Air}(h_{49} - h_{50}) = \dot{m}_{51}(h_{52} - h_{51}) + \dot{m}_{54} h_{54}$ $\dot{m}_{54} = \dot{m}_{Air}(w_{50} - w_{49})$ $\varepsilon_{dhum} = max\left\langle \left(\frac{h_{49} - h_{50}}{h_{49} - h_{50.ideal}}\right) . \left(\frac{\dot{m}_{52} h_{52} - \dot{m}_{51} h_{51} + \dot{m}_{54} h_{54}}{\dot{m}_{52} h_{52,ideal} - \dot{m}_{51} h_{51} + \dot{m}_{54} h_{54,ideal}}\right) \right\rangle$
Humidifier	$\dot{m}_{52} h_{52} - \dot{m}_{53} h_{53} = \dot{m}_{Air}(h_{48} - h_{47})$ $\dot{m}_{53} = \dot{m}_{52} - \dot{m}_{Air}(w_{48} - w_{47})$ $\varepsilon_{hum} = max\left\langle \left(\frac{h_{48} - h_{47}}{h_{48.ideal} - h_{47}}\right) . \left(\frac{\dot{m}_{52} h_{52} - \dot{m}_{53} h_{53}}{\dot{m}_{52} h_{52} - \dot{m}_{53} h_{53.ideal}}\right) \right\rangle$
TVC	$\eta_{TVC} = \frac{\dot{m}_{st,rev}}{\dot{m}_{st}}, \quad \dot{m}_{st} = \dot{m}_{46}$ $\dot{m}_{st,rev} s_{46} = \dot{m}_{Air}\left(s_{rev,49} - s_{48}\right) + \dot{m}_{56} s_{56}$ $\dot{m}_{st,rev} h_{46} = \dot{m}_{Air}\left(h_{rev,49} - h_{48}\right) + \dot{m}_{56} h_{56}$
Expander	$\eta_{TVC} = \frac{\dot{m}_{Air}(h_{50} - h_{47}) - \dot{m}_{55} h_{50}}{\dot{m}_{Air}\left(h_{50} - h_{s,47}\right) - \dot{m}_{55} h_{50}}$ $\dot{W}_{exp} = \dot{m}_{50} h_{50} - \dot{m}_{47} h_{47} - \dot{m}_{55} h_{55}$
High Pressure Pump	$\dot{W}_{hpp} = \dot{m}_{57}(h_{57} - h_{53})$ $\dot{W}_{hpp} = \dot{W}_{exp} + \dot{W}_{ert}, \quad \eta_{pu} = \frac{h_{57s} - h_{53}}{h_{57} - h_{53}}$
Energy recovery turbine	$\dot{W}_{ert} = \dot{m}_{59}(h_{59} - h_{60}), \quad \eta_{ert} = \frac{h_{360} - h_{60}}{h_{60} - h_{60}}$

3.3. Performance Criteria

The net power of the gas turbine is articulated as follows.

$$\dot{W}_{net,GT} = \dot{W}_{Gastur} - \dot{W}_{comp\,1} - \dot{W}_{comp\,2} \tag{31}$$

where, $\dot{W}_{Gastur}$, $\dot{W}_{comp\,1}$, and $\dot{W}_{comp\,2}$ are the produced power by gas turbine, Power consumed by compressors 1 and 2. The net output power of the devised system can be written as follows.

$$\dot{W}_{net,total} = \dot{W}_{net,GT} - \dot{W}_{WPump} \tag{32}$$

The gain output ratio (GOR) of the HDH-TVC-RO unit, MED unit, and the proposed integrated system is expressed as [23]:

$$GOR_{HDH-TVC-RO} = \frac{\dot{m}_{54} + \dot{m}_{55} + \dot{m}_{56} + \dot{m}_{58}}{\dot{m}_{46}} \tag{35}$$

$$GOR_{MED} = \frac{\dot{m}_{45}}{\dot{m}_{22}} \tag{35}$$

$$GOR_{total} = \frac{\dot{m}_{45} - \dot{m}_{61}}{\dot{m}_{22}} + \frac{\dot{m}_{54} + \dot{m}_{55} + \dot{m}_{56} + \dot{m}_{58}}{\dot{m}_{46}} \tag{35}$$

Another important metric in the setup is the Recovery Ratio (RR) which is which is defined as follows for the HDH-TVC-RO unit, the MED unit, and the proposed integrated system [23].

$$RR_{HDH-TVC-RO} = \frac{\dot{m}_{54} + \dot{m}_{55} + \dot{m}_{56} + \dot{m}_{58}}{\dot{m}_{51}} \tag{36}$$

https://doi.org/10.52202/069564-0168

$$RR_{MED} = \frac{\dot{m}_{45}}{\dot{m}_{11}} \quad (36)$$

$$RR_{total} = \frac{\dot{m}_{45} - \dot{m}_{61} + \dot{m}_{54} + \dot{m}_{55} + \dot{m}_{56} + \dot{m}_{58}}{\dot{m}_{11} + \dot{m}_{51}} \quad (36)$$

Finally, the Energy Utilization Factor (EUF) is defined as [27]:

$$EUF = \frac{\dot{W}_{net,total} + (\dot{m}_{45} - \dot{m}_{61})h_{45,fg} + \dot{m}_{54}h_{54,fg} + \dot{m}_{55}h_{55,fg} + \dot{m}_{56}h_{56,fg} + \dot{m}_{58}h_{58,fg}}{(\ LHV_{biomass} \times \dot{m}_{biomass} + \dot{Q}_{PTC,Hex}\ )} \quad (36)$$

4. Results and discussion

4.1. Model Comparison

In this subsection, a comparison between devised system (shown in Fig. 1) and the five different studies is carried out, and the results are illustrated in Table 3.

In the current research, we explore the utilization of solar energy and biomass gasifier as the primary energy sources, while employing the SCO_2 power cycle for efficient electricity generation. Moreover, we have incorporated multiple units, namely the MED, HDH-TVC, and RO, which collectively yield a substantial amount of freshwater. The proposed cycle exhibits impressive performance, with a power output of 4250 kW and a freshwater production rate of 29.36 kg/s. Notably, the recovery ratio, GOR, and EUF are reported as 23.74%, 14.38, and 3.372, respectively.

Comparatively, our findings demonstrate superior efficiency when contrasted with previous works. Table 3 illustrates that the GOR values and EUF values of prior studies range from 6.3 to 10.2 and from 0.516 to 0.884, respectively, further highlighting the enhanced performance of our present work.

Table 3: Model comparison between the reference system and the devised WT/HDH-MED-MVC system.

Ref.	Similar subsystems	Net output power (kW)	Freshwater rate (kg/s)	Recovery ratio (%)	GOR	EUF
Present study	Solar biomass, SCO2-MED, HDH-TVC-RO	4250	29.36	23.74	14.38	3.372
[8]	HDH-RO	4459	0.59	13.1	-	-
[30]	Solar, MED	419.2	6.8	26.01	8.5	0.884
[31]	SCO2-MED	290960	214.9	-	6.3	0.516
[32]	Biomass, GT, MED	220.4	0.48	-	-	0.55
[33]	Solar, MED-TVC	-	34.72	-	10.2	-

4.1. Basic results

For a base form of the study, the thermodynamic metrics of the devised system are presented in Table 4. The most important metrics include the mass flow rate of biomass, total freshwater distilled from the system, total GOR and EUF.

Table 4: Main thermodynamic metrics evaluated for the devised system.

$\dot{m}_{biomass}$	1.155 kg/s
$\dot{W}_{net,total}$	4250 kW
$\dot{m}_{fw,med}$	7.361 kg/s
$\dot{m}_{fw,HDH-TVC-RO}$	24.38 kg/s
$GOR_{HDH-TVC-RO}$	10.23
GOR_{MED}	6.133
GOR_{total}	14.38
RR_{MED}	26.73%
$RR_{HDH-TVC-RO}$	25.36%
RR_{total}	23.74%
EUF	3.372

4.1. Parametric Evaluation

In this section, the impact of the input vapor pressure to HDH-TVC and the compression pressure ratio are investigated on the main impressed performance criteria such as GOR, net output power and EUF for HDH-TVC-RO unit MED unit, and whole invented system.

4.1.1. Impact of the input vapor pressure to HDH-TVC on the system

Fig. 2 shows an alteration of the GOR, net output power, and EUF versus the input vapor pressure to HDH-TVC. As Fig. 2 (a) illustrates, in two subsystems of HDH-TVC-RO and MED, and in the entire system, the GOR is slightly increased with the increase in the input vapor to HDH-TVC. In the entire range of input vapor pressure to HDH-TVC changes from 40 to 60, the GOR value for the HDH-TVC-RO unit is higher than for the MED unit. Fig. 2 (b) shows the net output power as well as EUF versus the input vapor to HDH-TVC. As the input vapor pressure of HDH-TVC increases, the EUF value also increases almost linearly. Accordingly, the EUF value is almost 3.31 in input vapor pressure to HDH-TVC value of 40 and the value EUF increases until it reaches 3.42 at the input vapor pressure to HDH-TVC value of 60. On the other hand, the behaviour of net output power is parabolic in relation to the input vapor pressure to HDH-TVC. In this sense, as the input vapor pressure for HDH-TVC increases to 50, the net output power decreases and then increases.

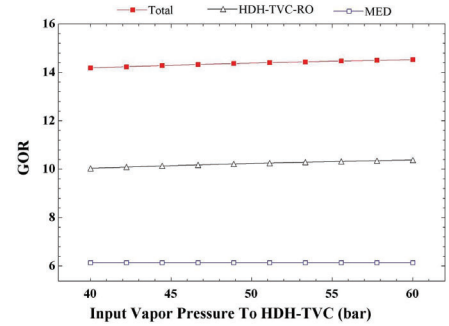

(a)

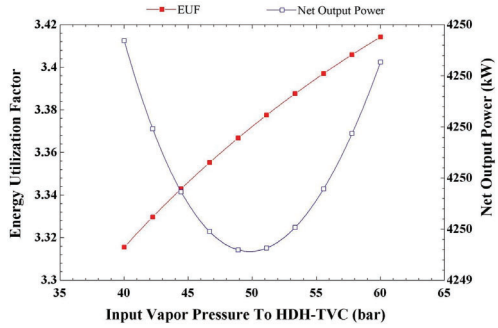

(b)

Figure 2: Impact of the input vapor pressure on HDH-TVC on the: (a) GOR, (b) EUF and net output power.

4.1.1. Impact of the pressure ratio of compressors on the system

Fig. 3 displays an alteration of the GOR, net output power, and EUF versus the pressure ratio of the compressors. As Fig. 3 (a) shows, the GOR of the MED subsystem remains almost constant and its value is equal to 6. In HDH-TVC-RO subsystem, the GOR remains constant and its value is equal to 10, similar to what we saw in MED subsystem. It is clear that in general the GOR of the HDH-TVC-RO subsystem is higher than that of the MED subsystem in the entire range of the pressure ratio of compressors. First, the total GOR increases with increasing pressure ratio of compressors. Its value reaches 15 at the pressure ratio of the compressors value of 3.7, then its value remains constant. Fig. 3 (b) shows the net output power as well as EUF versus pressure ratio of the compressors. The effect of pressure ratio changes on EUF is almost linear and the EUF is increased with increase of the pressure ratio of compressors. The EUF increases from 3.1 to 3.55, while the pressure ratio of the compressors varies from 2.2 to 4. The behavior pattern of net output power with the pressure ratio of compressors change is parabolic. The net output power starts from 4050 kW at the pressure ratio of compressors value of 2.2, and the net output power increases until it reaches its maximum (4250 kW) at the pressure ratio of compressors value of 3. Then the net output power decreases until it reaches 4125 kW at a compressor pressure ratio of 4.

https://doi.org/10.52202/069564-0168

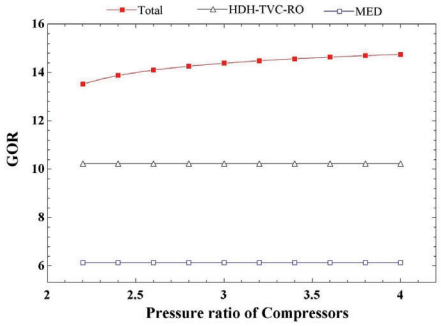

(a)

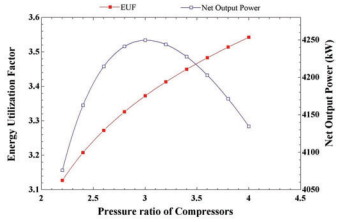

(b)

Figure 3: The impact of pressure ratio of compressors on the: (a) GOR, (b) EUF and net output power.

5. Concluding remarks

An integrated system with renewable resources is a matured solution to tackle the problems arising during the use of fossil fuels. On the other hand, to increase power production, SCO_2 cycles can be used, which have higher efficiency and the ability to drive a MED system. Consequently, in the present study, in addition to using the MED unit, the HDH-TVC-RO unit has also been used in the configuration. In regard to that, the following concluding points can be drawn:

- In the base mode, the fresh water rate, the GOR, and the EUF are 29.36 kg/s, 14.38, 3.372, respectively.
- The GOR of the HDH-TVC-RO unit is 40% higher than that of the MED unit, regardless of the value of input vapor pressure to HDH-TVC and pressure ratio of compressors.
- The total GOR of the developed system is constant and equal to 14.38 by changing vapor pressure to HDH-TVC.
- The total GOR enhances by increasing the pressure ratio of compressors
- The power generation process exhibits an interesting characteristic where an optimal point is reached when the pressure ratio of compressors is set to 3.
- The Energy Utilization Factor (EUF) experiences a notable improvement of 13.5% as the pressure ratio of compressors increases from 2.25 to 4.
- The EUF of the proposed cycle demonstrates a remarkable achievement, being nearly four times higher than that of previous works.

Nomenclature

Symbols		**Subscripts and superscripts**	
GT	Gas turbine	B	Brine
HTR	High Temperature Recuperator	CV	Control volume
LTR	Low Temperature Recuperator	da	dry air
MED	Multi effect desalination	Dhum	dehumidifier
RR	Recovery Ratio	Eff	Effect
EUF	Energy Utilization Factor	en	energy
LHV	Low Heat value $(kJ.kg^{-1})$	F	fuel
RO	Reverse Osmosis	FW	freshwater
HTR	High Temperature Recuperator	Hum	humidifier
LTR	Low Temperature Recuperator	in	inlet

GOR	Gained-Output-Ratio	max	maximum
h	specific enthalpy $(kJ.kg^{-1})$	net	net value
RO	Reverse Osmosis	out	outlet
$\dot{m}$	mass flow rate $(kg.s^{-1})$	pum	pump
N	Number of effects	ert	Energy recovery turbine
P	pressure (bar)	s	constant entropy
S	Salinity $(g.kg^{-1})$	SW	seawater
s	specific entropy $(kJ.kg^{-1}.K^{-1})$	tot	total
T	temperature (K)	v	vapor
TTD	terminal temperature difference(K)	w	work
$\dot{W}$	power (kW)	r	rated
$\dot{Q}$	Heat (kW)	rev	reversible
Greek Symbols		exp	Expander
ω	humidity ratio	hpp	High Pressure Pump
ε	Effectiveness (%)		
η	Efficiency (%)		

Acknowledgement

The present work was funded by the Silesian University of Technology for the beginning of scientific activities in a new research topic within the framework of project no. 32/014/SDU/10-22-37.

References

[1] A. Skorek-Osikowska, L. Bartela, D. Katla, and J.-L. Galvez-Martos, “Characteristic of a system for the production of synthetic natural gas (SNG) for energy generation using electrolysis, biomass gasification and methanation processes,” May 2019.

[2] M. A. Gonzalez-Salazar, T. Kirsten, and L. Prchlik, “Review of the operational flexibility and emissions of gas- and coal-fired power plants in a future with growing renewables,” *Renewable and Sustainable Energy Reviews*, vol. 82, pp. 1497–1513, Feb. 2018, doi: 10.1016/j.rser.2017.05.278.

[3] G. Xia, Q. Sun, X. Cao, J. Wang, Y. Yu, and L. Wang, “Thermodynamic analysis and optimization of a solar-powered transcritical CO2 (carbon dioxide) power cycle for reverse osmosis desalination based on the recovery of cryogenic energy of LNG (liquefied natural gas),” *Energy*, vol. 66, pp. 643–653, Mar. 2014, doi: 10.1016/j.energy.2013.12.029.

[4] A. Kouta, F. Al-Sulaiman, M. Atif, and S. bin Marshad, “Entropy, exergy, and cost analyses of solar driven cogeneration systems using supercritical CO2 Brayton cycles and MEE-TVC desalination system,” *Energy Convers Manag*, vol. 115, pp. 253–264, May 2016, doi: 10.1016/j.enconman.2016.02.021.

[5] P. Sharan, T. Neises, and C. Turchi, “Optimal feed flow sequence for multi-effect distillation system integrated with supercritical carbon dioxide Brayton cycle for seawater desalination,” *J Clean Prod*, vol. 196, pp. 889–901, Sep. 2018, doi: 10.1016/j.jclepro.2018.06.009.

[6] S. Alharbi, M. L. Elsayed, and L. Chow, “Thermo-Economic Analysis of an Integrated Supercritical CO2 Brayton Cycle and Multiple Effect Desalination Systems,” in *International Mechanical Engineering Congress and Exposition*, American Society of Mechanical Engineers, Nov. 2018. doi: 10.1115/IMECE2018-88409.

[7] P. Sharan, T. Neises, J. D. McTigue, and C. Turchi, “Cogeneration using multi-effect distillation and a solar-powered supercritical carbon dioxide Brayton cycle,” *Desalination*, vol. 459, pp. 20–33, Jun. 2019, doi: 10.1016/j.desal.2019.02.007.

[8] H. Rostamzadeh, S. Rostami, M. Amidpour, W. He, and D. Han, “Seawater Desalination via Waste Heat Recovery from Generator of Wind Turbines: How Economical Is It to Use a Hybrid HDH-RO Unit?,” *Sustainability*, vol. 13, no. 14, Jul. 2021, doi: 10.3390/su13147571.

[9] G. Wang, B. Dong, and Z. Chen, “Design and behaviour estimate of a novel concentrated solar-driven power and desalination system using S–CO2 Brayton cycle and MSF technology,” *Renew Energy*, vol. 176, pp. 555–564, Oct. 2021, doi: 10.1016/j.renene.2021.05.091.

 https://doi.org/10.52202/069564-0168

[10] L. Yuan, Q. Zhu, T. Zhang, R. Duan, and H. Zhu, “Performance evaluation of a co-production system of solar thermal power generation and seawater desalination,” *Renew Energy*, vol. 169, pp. 1121–1133, May 2021, doi: 10.1016/j.renene.2021.01.096.

[11] A. Omar, D. Saldivia, Q. Li, R. Barraza, and R. A. Taylor, “Techno-economic optimization of coupling a cascaded MED system to a CSP-sCO2 power plant,” *Energy Convers Manag*, vol. 247, p. 114725, Nov. 2021, doi: 10.1016/j.enconman.2021.114725.

[12] S. Khanmohammadi, S. Razi, M. Delpisheh, and H. Panchal, “Thermodynamic modeling and multi-objective optimization of a solar-driven multi-generation system producing power and water,” *Desalination*, vol. 545, p. 116158, Jan. 2023, doi: 10.1016/j.desal.2022.116158.

[13] S. Balafkandeh, V. Zare, and E. Gholamian, “Multi-objective optimization of a tri-generation system based on biomass gasification/digestion combined with S-CO2 cycle and absorption chiller,” *Energy Convers Manag*, vol. 200, p. 112057, Nov. 2019, doi: 10.1016/j.enconman.2019.112057.

[14] Y. Cao *et al.*, “Techno-economic investigation and multi-criteria optimization of a novel combined cycle based on biomass gasifier, S-CO2 cycle, and liquefied natural gas for cold exergy usage,” *Sustainable Energy Technologies and Assessments*, vol. 52, p. 102187, Aug. 2022, doi: 10.1016/j.seta.2022.102187.

[15] T. Hai, M. A. Ali, A. Alizadeh, S. F. Almojil, A. I. Almohana, and A. F. Alali, “Reduction in environmental CO2 by utilization of optimized energy scheme for power and fresh water generations based on different uses of biomass energy,” *Chemosphere*, vol. 319, p. 137847, Apr. 2023, doi: 10.1016/j.chemosphere.2023.137847.

[16] S. Khalilzadeh and A. Hossein Nezhad, “Utilization of waste heat of a high-capacity wind turbine in multi effect distillation desalination: Energy, exergy and thermoeconomic analysis,” *Desalination*, vol. 439, no. October 2017, pp. 119–137, 2018, doi: 10.1016/j.desal.2018.04.010.

[17] J. Bezaatpour, H. Ghiasirad, M. Bezaatpour, and H. Ghaebi, “Towards optimal design of photovoltaic/thermal facades: Module-based assessment of thermo-electrical performance, exergy efficiency and wind loads,” *Appl Energy*, vol. 325, Nov. 2022, doi: 10.1016/j.apenergy.2022.119785.

[18] Z. A. Zainal, R. Ali, C. H. Lean, and K. N. Seetharamu, “Prediction of performance of a downdraft gasifier using equilibrium modeling for different biomass materials,” *Energy Convers Manag*, vol. 42, no. 12, pp. 1499–1515, Aug. 2001, doi: 10.1016/S0196-8904(00)00078-9.

[19] A. Shokri Kalan, S. Heidarabadi, M. Khaleghi, H. Ghiasirad, and A. Skorek-Osikowska, “Biomass-to-energy integrated trigeneration system using supercritical CO2 and modified Kalina cycles: Energy and exergy analysis,” *Energy*, vol. 270, p. 126845, May 2023, doi: 10.1016/j.energy.2023.126845.

[20] T. Gholizadeh, M. Vajdi, and H. Rostamzadeh, “Exergoeconomic optimization of a new trigeneration system driven by biogas for power, cooling, and freshwater production,” *Energy Convers Manag*, vol. 205, p. 112417, Feb. 2020, doi: 10.1016/j.enconman.2019.112417.

[21] H. Ghiasirad, H. Rostamzadeh, and S. Nasri, “Design and Evaluation of a New Solar Tower-Based Multi-generation System: Part II, Exergy and Exergoeconomic Modeling,” in *Integration of Clean and Sustainable Energy Resources and Storage in Multi-Generation Systems*, Cham: Springer International Publishing, 2020, pp. 103–120. doi: 10.1007/978-3-030-42420-6_6.

[22] H. Ghiasirad, H. Rostamzadeh, and S. Nasri, “Design and Evaluation of a New Solar Tower-Based Multi-generation System: Part I, Thermal Modeling,” in *Integration of Clean and Sustainable Energy Resources and Storage in Multi-Generation Systems*, Cham: Springer International Publishing, 2020, pp. 83–102. doi: 10.1007/978-3-030-42420-6_5.

[23] S. Rostami, H. Ghiasirad, H. Rostamzadeh, A. S. Kalan, and A. Maleki, “A wind turbine driven hybrid HDH-MED-MVC desalination system towards minimal liquid discharge,” *S Afr J Chem Eng*, vol. 44, pp. 356–369, Apr. 2023, doi: 10.1016/J.SAJCE.2023.03.007.

[24] H. Rostamzadeh, H. Ghiasirad, M. Amidpour, and Y. Amidpour, “Performance enhancement of a conventional multi-effect desalination (MED) system by heat pump cycles,” *Desalination*, vol. 477, p. 114261, Mar. 2020, doi: 10.1016/j.desal.2019.114261.

[25] B. Stanek, W. Wang, and Ł. Bartela, “A potential solution in reducing the parabolic trough based solar industrial process heat system cost by partially replacing absorbers coatings with non-selective ones in initial loop sections,” *Appl Energy*, vol. 331, p. 120472, Feb. 2023, doi: 10.1016/j.apenergy.2022.120472.

[26] F. A. Al-Sulaiman, G. Prakash Narayan, and J. H. Lienhard, “Exergy analysis of a high-temperature-steam-driven, varied-pressure, humidification–dehumidification system coupled with reverse osmosis,” *Appl Energy*, vol. 103, pp. 552–561, Mar. 2013, doi: 10.1016/j.apenergy.2012.10.020.

[27] H. Ghiasirad, N. Asgari, R. Khoshbakhti Saray, and S. Mirmasoumi, “Thermoeconomic assessment of a geothermal based combined cooling, heating, and power system, integrated with a humidification-

dehumidification desalination unit and an absorption heat transformer," *Energy Convers Manag*, vol. 235, p. 113969, 2021, doi: https://doi.org/10.1016/j.enconman.2021.113969.

[28] A. Shekari Namin, H. Rostamzadeh, and P. Nourani, "Thermodynamic and thermoeconomic analysis of three cascade power plants coupled with RO desalination unit, driven by a salinity-gradient solar pond," *Thermal Science and Engineering Progress*, vol. 18, p. 100562, Aug. 2020, doi: 10.1016/j.tsep.2020.100562.

[29] A. S. Kalan, H. Ghiasirad, R. K. Saray, and S. Mirmasoumi, "Thermo-economic evaluation and multi-objective optimization of a waste heat driven combined cooling and power system based on a modified Kalina cycle," *Energy Convers Manag*, vol. 247, Nov. 2021, doi: 10.1016/j.enconman.2021.114723.

[30] E. D. Kerme *et al.*, "Energetic and exergetic performance analysis of a solar driven power, desalination and cooling poly-generation system," *Energy*, vol. 196, p. 117150, Apr. 2020, doi: 10.1016/j.energy.2020.117150.

[31] S. Alharbi, M. L. Elsayed, and L. C. Chow, "Exergoeconomic analysis and optimization of an integrated system of supercritical CO2 Brayton cycle and multi-effect desalination," *Energy*, vol. 197, p. 117225, Apr. 2020, doi: 10.1016/j.energy.2020.117225.

[32] Z. K. Mehrabadi and F. A. Boyaghchi, "Exergoeconomic and exergoenvironmental analyses and optimization of a new low-CO2 emission energy system based on gasification-solid oxide fuel cell to produce power and freshwater using various fuels," *Sustain Prod Consum*, vol. 26, pp. 782–804, Apr. 2021, doi: 10.1016/j.spc.2020.12.041.

[33] A. Khouya, "4E assessment of a hybrid RO/MED-TVC desalination plant powered by CPV/T systems,"CPV / T systems', *Energy Convers Manag*, vol. 277, p. 116666, Feb. 2023, doi: 10.1016/j.enconman.2023.116666.

 https://doi.org/10.52202/069564-0168